CONFERENCE PRE-PRINT

TRANSPORT PROPERTIES OF TRAPPED-ELECTRON-MODE TURBULENCE INTERACTING WITH TEARING MODES IN TOKAMAK PLASMAS

Yifan YAN, Jiquan LI*, Haotian CHEN
Southwestern Institute of Physics (SWIP)
Chengdu 610041, China

*Email: lijq@swip.ac.cn

Abstract

This study investigates a novel transport property in trapped electron mode (TEM) turbulence interacting with dynamically evolving magnetic islands (MIs) generated by the resistive tearing mode (RTM). These interactions were simulated using a compact gyro-Landau-fluid model incorporating trapped electron dynamics. In a regime where both the temperature gradient-driven TEM (∇T_e-TEM) and RTM instabilities exhibit moderate strength, the resulting multi-scale TEM-RTM turbulence exhibits oscillatory particle and heat fluxes. Specifically, turbulent electron heat flux bursts periodically, synchronized with the recurrent excitation of m/n=2/1 MIs, where m and n represent the poloidal and toroidal mode numbers, respectively. The underlying physical mechanisms are analyzed by examining the transport response to the dynamic MIs. Results demonstrate the periodic excitation of the 2/1 mode, accompanied by alternating phases of magnetic reconnection and island shrinkage, leading to cyclic state transitions of the n=1 RTM eigenmodes. Concurrently, the 3/1 mode, characterized by nearly stationary MIs of a specific width, plays a crucial role in modulating these cycles via toroidal mode coupling with the adjacent 2/1 mode. These findings offer new insights into the understanding of transport intermittency and oscillatory transport phenomena observed in tokamak plasmas containing dynamic MIs, and may provide a connection to experimental observations.

1. INTRODUCTION

The complex, multi-scale interplay between macroscopic magnetohydrodynamic (MHD) instabilities and microscopic drift-wave turbulence is a fundamental characteristic of magnetically confined plasmas, with significant implications for confinement in fusion devices. For instance, tearing modes (TMs) can nonlinearly interact with turbulence—such as that driven by the ion temperature gradient (ITG) mode and trapped electron modes (TEMs)—to regulate turbulent transport. Furthermore, as TMs evolve, large-scale magnetic islands (MIs) can form via magnetic reconnection. These islands can distort the equilibrium magnetic topology, generating radial magnetic field perturbations that enhance the transport of particles and heat, thereby degrading overall confinement.

Previous nonlinear studies of resistive TMs (RTMs) and ITG turbulence, conducted using fluid models in simplified slab geometry, have provided initial insights into this multi-scale physics [1]. Subsequent work has incorporated static magnetic islands into toroidal drift-wave turbulence to explore more realistic interactions, addressing the complex coupling through both nonlinear spectral and linear geometric effects [2]. However, the assumption of static islands precludes any analysis of their dynamic response to turbulence or their feedback upon it. Self-consistent simulations that capture the co-evolution of MHD instabilities and micro-turbulence are therefore essential for further progress.

Experimentally, the coexistence of MHD islands and TEM turbulence—primarily driven by the electron temperature gradient—has been clearly observed [3]. Analyses of electron transport in response to island dynamics, based on measured temperature fluctuations, have revealed intermittent or oscillatory behavior linked to interactions between turbulence and the evolving magnetic topology [4, 5]. While turbulence spreading into the island region is often proposed as the dominant mechanism, other pathways require deeper investigation.

This study employs a gyro-Landau-fluid model, which self-consistently incorporates trapped electron dynamics through the Weiland closure [6, 7], to simulate the nonlinear interaction between TEM turbulence and a resistive tearing mode (RTM). We investigate the saturation of TEM turbulence, the dynamics of the magnetic island, and their combined impact on transport. Specifically, turbulent electron heat flux bursts periodically, synchronized with the recurrent excitation of m/n=2/1 MIs, leading to a cyclic transition of the n=1 RTM eigen state (where m and n are the poloidal and toroidal mode numbers, respectively).

2. PHYSICAL MODEL AND NUMERICAL APPROACH

Building upon pioneering reduced fluid models that incorporate gyro-Landau-fluid closures and the Weiland model for trapped electron dynamics [6-9], we leverage their capability to capture essential physics—such as Landau damping and trapped electron effects in plasma turbulence—to establish a six-field electromagnetic (EM) fluid model [9-11]. The model equations are:

$$d_t n_e = f_c\omega_{de}(n_0\phi - p_e) + f_t\omega_{dte}(n_0\phi - p_e) - f_c(n_0\nabla_\parallel v_\parallel - \nabla_\parallel J) + D_n\nabla_\perp^2 n_e \quad , \tag{1}$$

$$d_t T_e = T_{e0}\left[\lambda_{e1}\omega_{dte}\phi + (\Gamma - 1)T_{e0}\omega_{dte}\, n_e/n_0 + \lambda_{e2}\omega_{dte}T_e\right] + D_{Te}\nabla_\perp^2 T_e \quad , \tag{2}$$

$$d_t\nabla_\perp^2\phi = -T_{i0}a[\partial_r \ln n_0 + \partial_r \ln T_{i0}]\partial_\theta\nabla_\perp^2\phi + \frac{\nabla_\parallel J}{n_0} - \omega_{di}(n_0\phi + p_i)$$

$$+ f_c\omega_{de}(n_0\phi - p_e) + f_t\lambda_{e3}\omega_{dte}(n_0\phi - p_e) + \mu\nabla_\perp^4\phi \quad , \tag{3}$$

$$d_t v_\parallel = -(f_c T_{e0}\nabla_\parallel n_e + \nabla_\parallel p_i)/n_0 + D_{\mathrm{v}}\nabla_\perp^2 v_\parallel \quad , \tag{4}$$

$$\beta d_t A_\parallel = -\nabla_\parallel\phi + \nabla_\parallel p_e/n_0 + \sqrt{\pi\tau m_e/2m_i}\,\left|\nabla_\parallel\right|(v_\parallel - J/n_0) - \eta J \, , \tag{5}$$

$$d_t T_i = T_{i0}[(\Gamma - f_c)\omega_{di}\phi + (2\Gamma - f_c)\omega_{di}T_i + T_{i0}(\Gamma - f_c)\omega_{di}\, n_e/n_0] - f_t T_{e0}\omega_{dte}(\phi - p_e/n_0)$$

$$-\Gamma T_{i0}\nabla_\parallel v_\parallel + f_c T_{i0}(\nabla_\parallel v_\parallel - \nabla_\parallel J/n_0) - \lambda_{i0}\sqrt{8T_{i0}/\pi}\,\left|\nabla_\parallel\right|T_i + D_{T_i}\nabla_\perp^2 T_i \quad . \tag{6}$$

Here, $n_e, T_e, \nabla_\perp^2\phi, v_\parallel, A_\parallel$ and T_i denote the total electron density, electron temperature, vorticity, parallel ion velocity, parallel magnetic vector potential (note that $A_\parallel$ corresponds to the negative magnetic flux ψ), and ion temperature, respectively. The parallel current is defined by Ampère's law as $J = -\nabla_\perp^2 A_\parallel$. All other physical quantities are defined consistently with Refs. [9-11]. This compact model, which self-consistently integrates RTM and TEM turbulence, was finalized by optimizing several numerical coefficients (e.g., λ_{i0}, λ_{ej}, here, j =1, 2, 3). These coefficients were carefully calibrated to ensure that the linear eigenmodes—including real frequency, growth rate, and mode structure—are benchmarked against gyrokinetic (GK) models with an acceptable degree of accuracy.

The model equations are solved as an initial-value problem using the newly developed global Extended Fluid Code (ExFC), designed for tokamak geometry. The computational domain is defined by normalized radial (r), poloidal (θ), and toroidal (φ) coordinates, typically spanning $[L_r, L_\theta, L_\varphi] \approx [a, 2\pi, 2\pi]$ To enhance numerical accuracy and efficiency, the radial domain is restricted to $r \in [0.1a, a]$. The domain is discretized on a 3D grid of size $(N_r, N_\theta, N_\varphi)$. Dirichlet boundary conditions are applied in the radial direction, while periodic conditions are used poloidally and toroidally.

The initial equilibrium plasma profiles correspond to the standard Cyclone Base Case (CBC). The density and temperature profiles are given by: $F_0(r) = F_c\exp\{-(\triangle_{Fr}/L_F)\tanh[(r - r_0)/\triangle_{Fr}]\}$, where F denotes either density or temperature, and the subscript c indicates the value at the plasma center. The safety factor profile is prescribed as $q(r) = q_0 + q_a(r/a)^4$. The parameters used are $r_0 = 0.5a$, $\triangle_{Fr} = 0.3a$, $q_0 = 1.75$.

3. NONLINEAR SIMULATION

3.1 Multi-mode Turbulence Interaction

Simulations are performed to investigate the interaction between electrostatic TEM turbulence and RTMs, where MIs naturally arise. Simulation parameters—plasma β, resistivity, viscosity, electron temperature gradient, and safety factor q-profile—were tuned to realize a strongly unstable ∇T_e-driven TEM coexisting with a weakly unstable RTM. For a representative case, Fig. 1 plots the temporal evolution of volume-averaged potential energy $\langle\phi_n^2\rangle/2$ and magnetic energy $\langle\psi_n^2\rangle/2$ for dominant RTMs (n = 1, 2), most unstable TEMs (n = 8–10), and zonal modes (m/n = 0/0), revealing three phases.

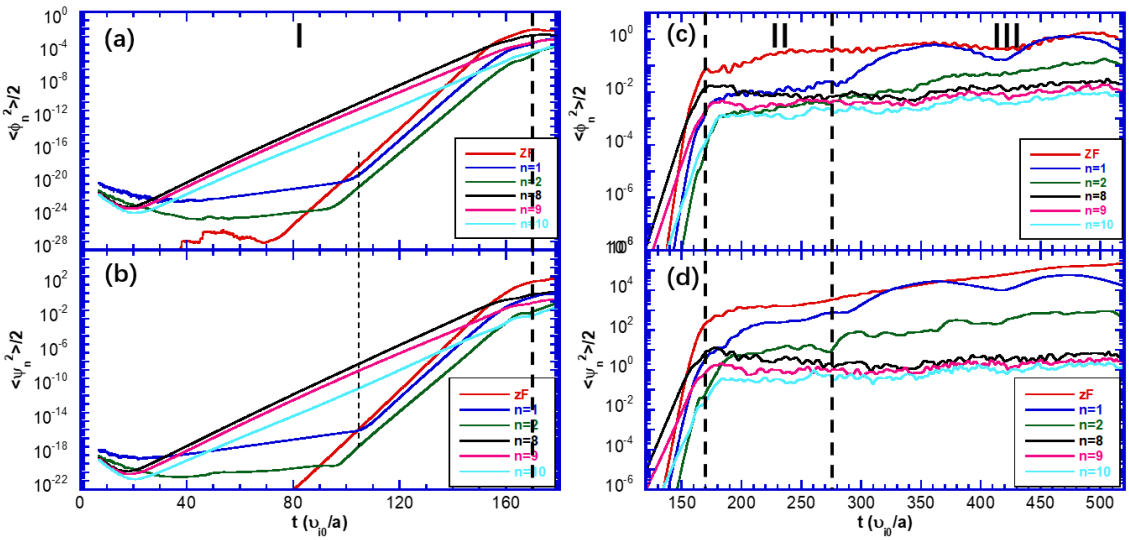

FIG.1 Temporal evolution of fluctuating potential energy $\langle\phi_n^2\rangle/2$ (a) and magnetic energy $\langle\psi_n^2\rangle/2$ (b) for dominant modes, including RTMs (n=1,2), TEMs (n=8–10), and the zonal mode (n=0). Other simulation parameters are set as $a = 100$, $\varepsilon = 0.36$, $\beta = 0.2\%$, $\eta = 0.01$, and $D_n = D_{Te} = \mu = D_v = D_{Ti} = 0.05$.

Phase I: TEM turbulence grows linearly. The n = 1 RTM displays two-stage dynamics: a weak linear instability, followed by forced growth at roughly twice the dominant TEM growth rate. Zonal modes grow at a similar doubled rate. This enhancement arises from nonlocal NMC in spectral space, consistent with turbulently driven magnetic reconnection [12,13].

Phase II: The TEM amplitude saturates and slightly decreases, while RTM energy rises, accompanied by the emergence of small 2/1 islands (Fig. 2). Energy transfer from TEM to RTM via nonlocal NMC is indicated by a TEM spectral peak downshift and a spectral gap between RTM- and TEM-dominated ranges (Fig. 3). Instantaneous potential contours (Fig. 4) show that, as NMC proceeds, 2/1 islands form and initially reduce turbulence inside the island near q = 2. Later, turbulence spreads into the island. The 3/1 RTM remains too weak to affect dynamics in the 2/1 region.

Phase III: The system enters an oscillatory regime where RTMs repeatedly grow and decay. The 2/1 RTM nears locking and dominates EM fluctuations; large-scale potential vortices form and regulate the ambient TEMs. Magnetic reconnection and subsequent 2/1 island shrinkage alternate (Fig. 2), while the 3/1 island width remains nearly constant after a turning point.

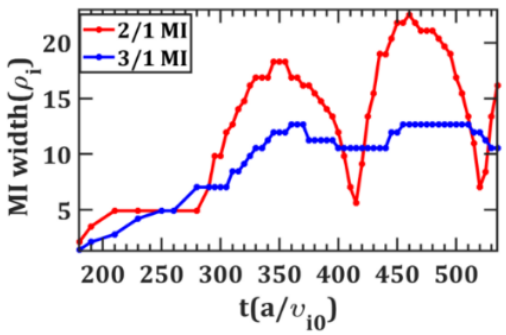

FIG.2 Temporal evolution of the 2/1 and 3/1 MI widths during Phases II and III. Here, the MI width is defined as the radial distance between the inner and outer separatrix surfaces in the O-point region.

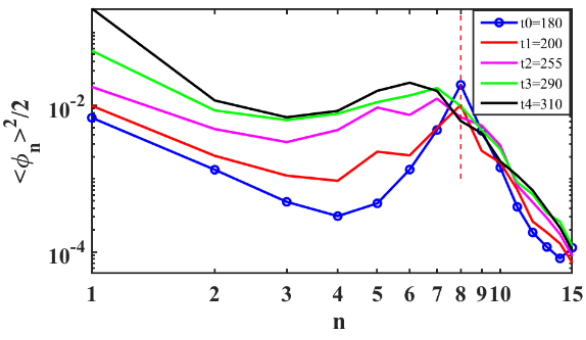

FIG.3 Temporal evolution of EM turbulence spectral distribution versus toroidal mode number n in Phase II and early Phase III.

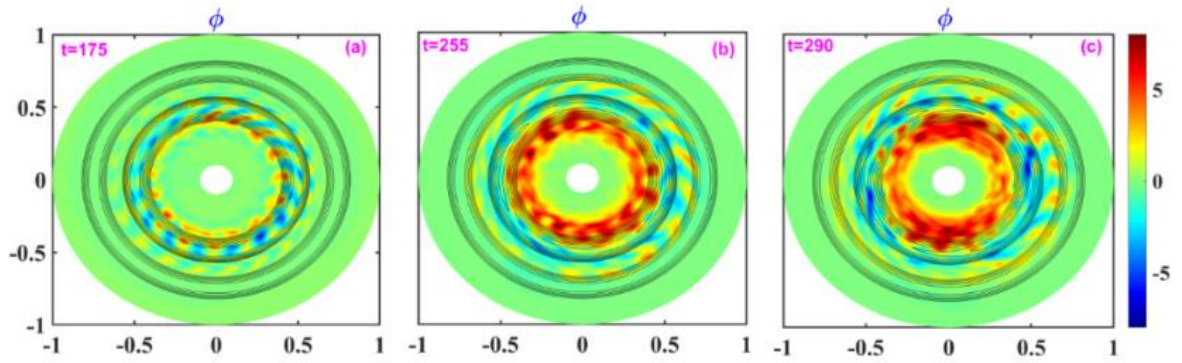

FIG.4: Evolution of fluctuating potential contour plots accompanying the 2/1 and 3/1 MI structures in Phase II.

To diagnose Phase III, we decompose n = 1 and n = 2 RTMs poloidally. The 2/1 component drives the oscillations in n = 1 energy (Fig. 5); the 3/1 island is nearly stationary once its width saturates. Growth of the 2/1 mode corresponds to reconnection and island widening ("MIs growing stage"), while decline corresponds to island shrinkage ("MIs shrinking stage"). The 3/1 growth lags the 2/1, implying TMC that enhances reconnection and destabilizes both modes. Radial structures (Fig. 6) show that, early in Phase I, the linear n = 1 mode has an eigen state, which is characterized by a hump-shaped 3/1 component and a fixed, smaller 3/1 to 2/1 amplitude ratio, namely the eigen structures. In Phases II–III, nonlocal NMC strengthens the n = 1 RTM; when islands are small, the 3/1 potential amplitude becomes comparable to 2/1 (Figs. 6b, d, f), enabling stronger TMC. When the 2/1 width peaks, the n = 1 mode reverts toward its eigenmode structure (Figs. 6c, e).

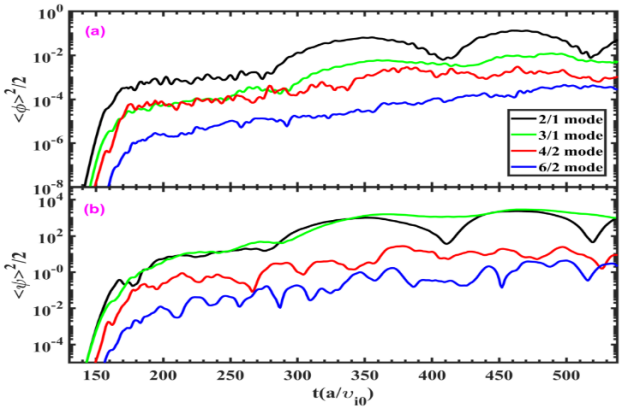

FIG.5 Temporal evolution of fluctuating potential energy $\langle\phi_{m,n}^2\rangle/2$ (a) and magnetic energy $\langle\psi_{m,n}^2\rangle/2$ (b) for dominant poloidal components of the RTMs (n=1,2).

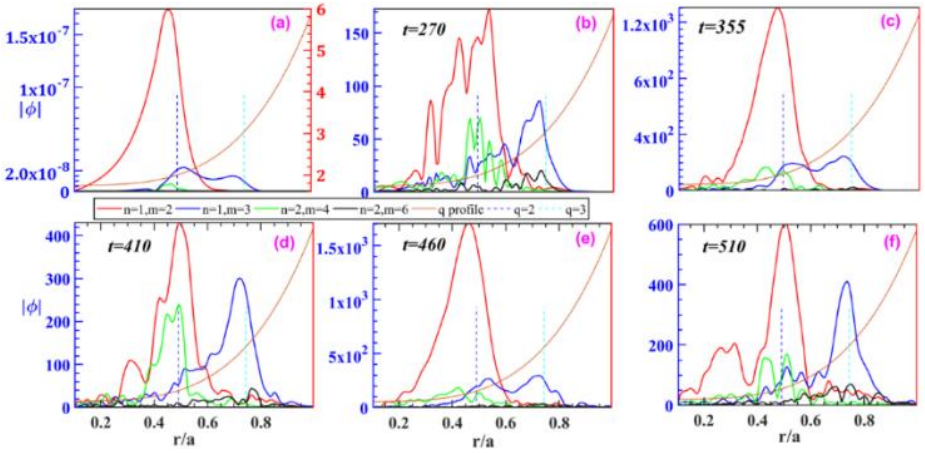

FIG.6 Temporal evolution of the radial structures of the 2/1 and 3/1 RTM components. The dashed lines denote the q=2 and q=3 magnetic surfaces.

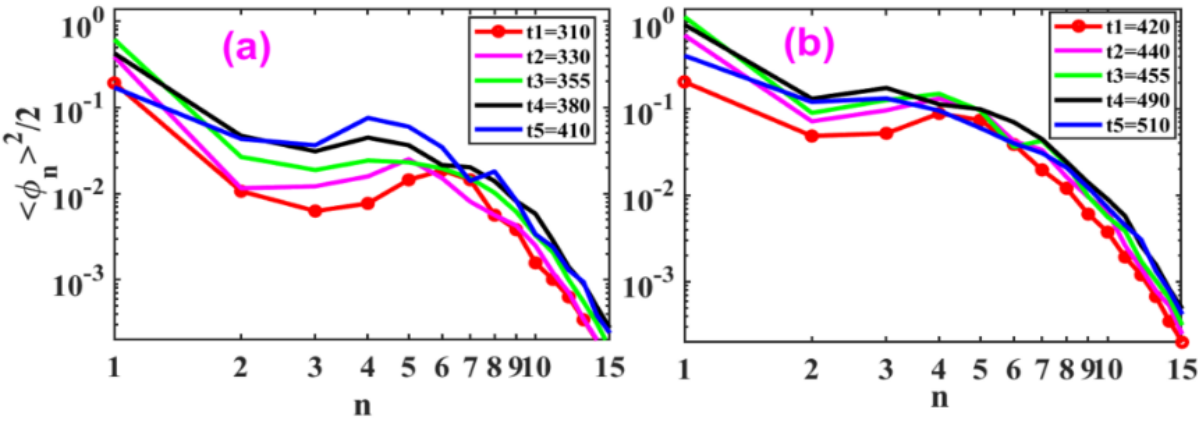

FIG.7 Temporal evolution of EM turbulence spectral distribution versus toroidal mode number n during the first oscillation cycle (a) and the next one (b).

Mechanism of alternating reconnection and shrinkage: Initially, nonlocal NMC destabilizes the 2/1 mode, producing turbulence-driven reconnection and island growth; TMC with 3/1 further reinforces both islands (Figs. 6a–c). As 2/1 islands rotate slowly in the electron diamagnetic direction, phase self-adaptation tends toward the RTM eigenmode phase relation, while inverse TEM energy cascade shifts the TEM spectral peak downward (Fig. 7a). Nonlocal NMC boosts n = 1 spectral energy from t_1 to t_3, with maximal 2/1 width and amplitude at t = 355. Subsequently, back-reaction from the 2/1 mode (island plus vortices) modulates TEMs via nonlocal NMC, transferring energy back to TEM turbulence and inducing island shrinkage (t_3–t_5, Fig. 7a). By the end of the first cycle, the 2/1 island nearly disappears, whereas 3/1 persists (Fig. 2), consistent with distinct drive/damping: 3/1 is sustained by TMC and damped by viscosity; 2/1 is more sensitive to nonlocal NMC and phase matching. In subsequent cycles, 2/1 is re-excited by NMC and destabilized by TMC with the residual 3/1. Over multiple cycles, the spectral gap between high-n TEMs and low-n MHD modes can be bridged, forming a quasi-steady multi-mode, multi-scale EM spectrum (Fig. 7b).

3.2 Oscillatory Transport Behavior

The multi-scale EM turbulence modifies the initial profiles through transport tied to turbulent structure and saturation. We evaluate the turbulent particle flux $\Gamma_{ne} = \langle \tilde{n}_e \cdot \tilde{v}_r \rangle$and ion/electron heat fluxes $Q_{i,e} = \langle \tilde{T}_{i,e} \cdot \tilde{v}_r \rangle$, with $\tilde{v}_r$ from the electrostatic $E \times B$ flow. β scans indicate negligible EM contributions to ion transport, while electron thermal and particle transport from magnetic flutter are small at low-to-moderate β ($\beta \lesssim 0.25\%$) yet remain computationally challenging to resolve accurately [14].

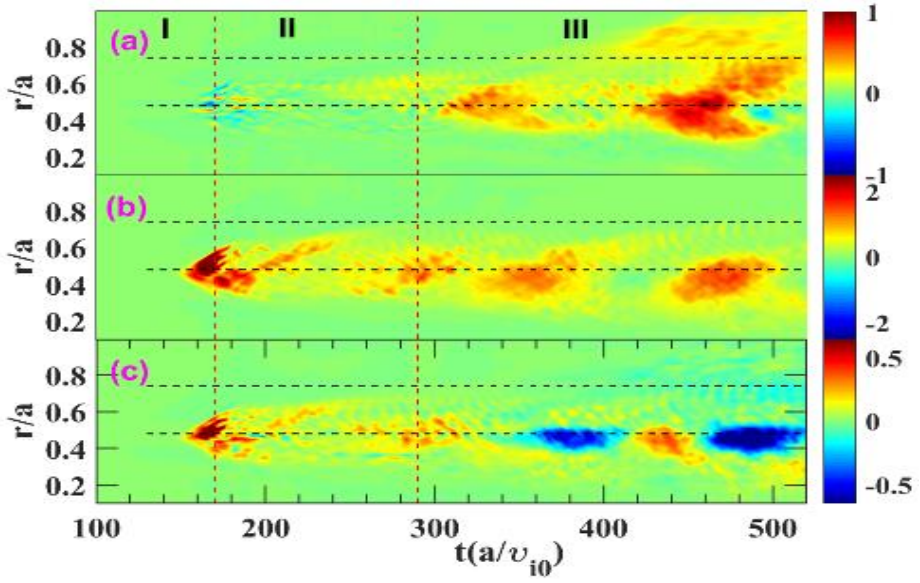

FIG.8 Spatiotemporal evolution of the turbulent particle flux (a), electron heat flux (b) and ion heat flux (c).

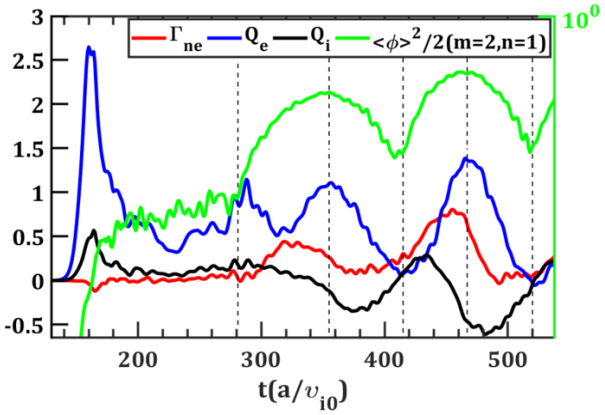

FIG.9 Temporal evolution of radially-averaged fluxes Γ_{ne} and $Q_{i,e}$ in the 2/1 MIs region. Temporal evolution of the 2/1 mode's potential energy is also plotted for comparison.

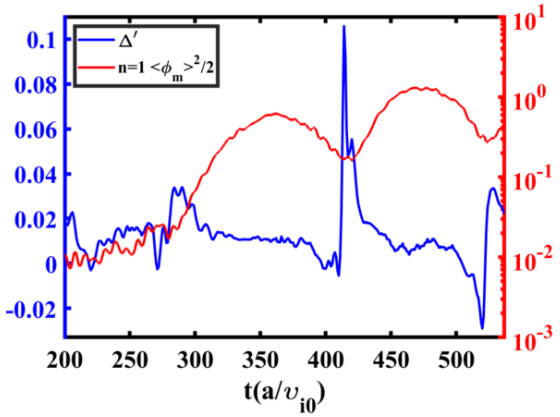

FIG.10: Temporal evolution of the RTM instability parameter (Δ') at the position of q=2 surface in Phase II and III of the simulation shown in FIG.1.

Figure 8 shows spatiotemporal patterns of Γ_{ne}, Q_e, and Q_i, revealing pronounced oscillatory bursts localized near the 2/1 island radius, attributable to convective transport by large-scale vortices. Radially averaged signals (Fig. 9) exhibit fixed phase relations: electron and ion heat fluxes are out of phase, with ion bursts lagging electrons.

Electron heat transport: The oscillatory Q_e is synchronous with alternating reconnection and island shrinkage (Fig. 9), demonstrating coupling to magnetic topology. Enhanced 2/1 RTMs (larger islands) increase Q_e via (1) convective transport by large-scale MHD vortices and (2) TEM-driven turbulent transport, amplified through nonlocal cross-phase modulation with RTMs. The Q_e peaks coincide with large island width and RTM eigenstate vortex flows.

Figure 10 shows Δ′(q = 2) during Phases II–III, treating mean nonlinear profiles as quasi-equilibria. Positive Δ′ spikes suggest a linear contribution to early reconnection, subsequently reinforced by periodically excited turbulence-driven islands. Quasi-linear gradient scale lengths L_n/R, L_{Te}/R, L_{Ti}/R (Fig. 11) show partial T_e flattening in Phase II and full flattening or reversal within large islands, indicating that enhanced Q_e stems from nonlinear RTM–TEM interactions rather than increased linear drive from profile changes.

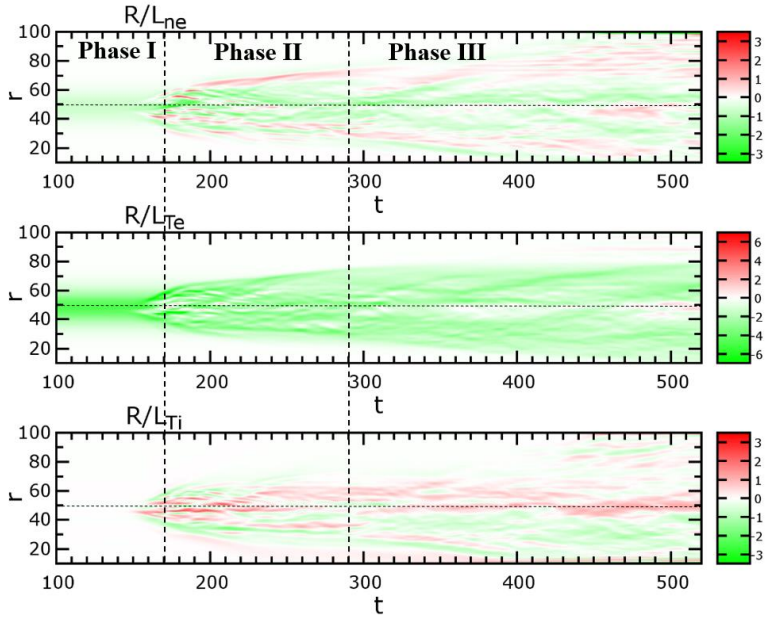

FIG.11 Temporal evolution of the quasi-linear equilibrium gradient scale lengths of electron particle (R/L_n) and temperature (R/L_{te}) as well as ion temperature (R/L_{ti}) corresponding to the simulation in Fig.1.

Ion heat transport: Q_i alternates between inward pinch and outward diffusion without significant background ITG turbulence. Low ion transport in Phase II reflects weak RTMs and TEM-dominated electron transport. In Phase III, Q_i oscillations track 2/1 island dynamics. The origin of the initial phase offset between Q_i and Q_e remains an open question.

Particle transport: Particle flux exhibits similar oscillatory behavior without a clear particle pinch, likely influenced by the initial density gradient, which also drives TEMs. Overall, TEM turbulence sets the mean electron heat transport level in Phase II, while RTM fluctuations govern the oscillatory amplitude and phasing in Phases II–III.

3.3 Analysis of Transport Characteristics

The alternating reconnection–shrinkage and oscillatory transport persist across moderate ranges of ∇T_e, β, resistivity, and viscosity. A qualitative trend—pending full scans—is that oscillations weaken when TEM or RTM activity is either too strong or too weak. The oscillation amplitude is small when the 3/1 RTM is weak (e.g., lower resistivity and/or higher viscosity), underscoring the essential role of TMC between 2/1 and 3/1 modes in setting island dynamics within TEM–RTM interacting EM turbulence.

In realistic tokamak plasmas, ∇n_e-driven TEMs and/or ITG modes can dominate electrostatic turbulence, while low-n MHD activity (e.g., neoclassical tearing modes, fishbones, TAEs) can seed islands. Such multi-mode systems admit diverse eigenmodes and scales, making nonlinear interactions and resulting transport highly complex and worthy of further study. Some key issues on the transport characteristics are analyzed as follows:

Transport oscillation frequency (TOF): The TOF of Γ_e, Q_e, and Q_i matches the alternation frequency of 2/1 reconnection–shrinkage. Although theory is challenging and simulations cannot span all parameters, typical cycles yield $\Delta t \approx 115$ with small RMS variation, giving $\omega_{TOF} = 2\pi/\Delta t \approx 0.055$. During oscillations, the TEM spectral peak downshifts from n = 8–10 to n = 3–4 by inverse energy cascade. The trapped-electron precession frequency $\omega_{*dte} \approx 0.05$–$0.067$ for n = 3–4, suggesting TOF $\approx \omega_{*dte}$. This is plausible if trapped-electron precession in TEMs resonates with the n = 1 RTM helical structure (2/1 island), implying a wave–particle resonance manifesting as a wave–wave resonance in Landau or gyro-Landau fluid closures. Caution is warranted, as the agreement could be coincidental and requires verification.

Role of 3/1 islands: With higher resistivity, both 2/1 and 3/1 widths grow; the 3/1 island then saturates at a nearly fixed width in the first cycle and persists, being mainly viscosity-damped. Coupled via TMC, the quasi-stationary 3/1 island likely contributes to the alternation of reconnection and shrinkage. The combined axisymmetric field with a static helical 3/1 component resembles a stellarator-like configuration. Experimental observations in LHD show bifurcation between island healing and growth [14, 4, 5], interpretable via tokamak island formalisms. We hypothesize that TEM–RTM interactions can upset torque and width-balance relations, producing spontaneous island growth or healing depending on shear, β, and collisionality (resistivity/viscosity).

Zonal modes: Zonal flow (electrostatic) and zonal current (magnetic) reshape profiles and can suppress primary instabilities. In Fig. 1, MI dynamics more strongly govern multi-mode interactions and transport oscillations. During Phase II, the zonal flow grows exponentially in the first half, while the zonal magnetic field grows in the latter half. Theory indicates zonal flow drive by nonlocal cross-phase modulation (four-wave modulational instability in electrostatic turbulence or parametric three-wave in finite-β EM turbulence). The zonal flow saturates at an amplitude much smaller than the zonal magnetic field and is weaker in MHD-dominated dynamics like RTMs. The zonal current is crucial to trigger reconnection and island formation. In Phase III, the zonal flow evolves to a quasi-steady state that appears decoupled from island dynamics and the zonal magnetic field. Given the dominant role of islands here, we defer a full treatment of zonal flow dynamics to future work.

4. SUMMARY AND DISCUSSION

This study investigates how turbulent transport couples with magnetic topology via MIs in tokamak plasmas. Using an alternative reduced gyro-Landau-fluid model including trapped electron dynamics, we simulate nonlinear interactions between electrostatic, ∇T_e-driven TEM turbulence and weak MHD RTMs. Transport is analyzed from the spatiotemporal structure of EM fluctuations, including magnetic reconnection and island shrinkage.

We identify three phases of EM turbulence: linear growth (I), TEM-saturated state (II), and RTM-dominated quasi–steady state (III). From I→II, TEM saturates through inverse cascade and back-reaction from force-

enhanced RTMs and zonal modes via nonlocal NMC/modulation. In II, RTMs and MIs grow slowly while TEM weakens slightly; coupling remains weak, indicating stabilization by small MIs. As RTMs strengthen via nonlocal NMC, TMC between 2/1 and 3/1 modes destabilizes RTMs and drives Phase III, with coexisting dominant RTMs (with dynamic MIs) and ambient TEM.

The transport response exhibits oscillatory behavior. Electron heat flux shows regular bursts synchronized with 2/1 MI reconnection and subsequent island shrinkage. Ion heat flux alternates between outward diffusion and inward thermal pinch; under stronger RTM drive, it becomes predominantly inward with oscillations. Meanwhile, radially diffusive electron particle and heat fluxes increase on average. The oscillation timescale matches the trapped-electron precession drift frequency. Burst amplitude depends on the relative TEM vs RTM drive, linked to profiles and parameters such as β, resistivity, and viscosity.

Mechanistically, the 2/1 mode is periodically excited, cycling between reconnection (growth) and shrinkage, implying repeated state transitions of the n=1 RTM eigenmodes. The 3/1 mode, with nearly stationary MIs of fixed width, modulates these cycles via TMC with the adjacent 2/1 mode, effectively pacing the oscillations.

The simulated transport oscillations are qualitatively consistent with observations in DIII-D and KSTAR [15, 4,5], where non-rotating 2/1 MIs are locked by externally applied RMPs to avoid disruptions. There, MI dynamics can be captured by tearing-mode theory (e.g., Rutherford evolution), and turbulence spreading has been proposed as a contributor to oscillatory transport. In our simulations, the 2/1 MIs appear nearly locked by the 3/1 MIs, analogous to an RMP, and this locking governs the transport oscillation tied to alternating reconnection and shrinkage. While turbulence spreading into MIs is present, it is not dominant in setting transport. Further validation and model verification are needed, but these results offer a new perspective on oscillatory transport linked to MI dynamics in multi-mode tokamak turbulence.

ACKNOWLEDGEMENTS

This work was supported by the National Key R & D Program of China with grant Nos. 2024YFE03020001, 2024YFE03230300, 2022YFE03010004, National Natural Science Foundation of China with grant Nos. 12275071 and 12375213. It was also partially supported by Innovation Program of Southwestern Institute of Physics (Grants No. 202301XWCX001) and Science and technology project of Sichuan Province with grant Nos. 2025ZNSFSC0061 and 2023ZYD0016.

REFERENCES

[1] Li J Q et al. 2014 Phys. Plasmas 21 020703

[2] Hornsby W A *et al* 2011 Plasma Phys. Control. Fusion 53 054008

[3] Jiang M *et al* 2020 *Nucl. Fusion* 60 066006

[4] Choi M J et al 2021 Nature communications 12 375

[5] Ida K et al 2015 Scientific reports 5 16165

[6] Kinsey J E et al 2008 Phys. Plasmas 15 055908

[7] Weiland J et al 2007 Plasma Phys. Control. Fusion 49 A45

[8] Waltz R E et al. 1997 Phys. Plasmas 4 2482

[9] Garbet X et al 2003 Phys. Rev. Lett 91 035001.

[10] Miyato N. Li J.Q. and Kishimoto Y., Nucl. Fusion **45**, 425 (2005).

[11] Li J Q et al 2020 IAEA Fusion Energy Conf. (Nice, France) TH/pp P7–21.

[12] Dubuit N., et al 2021 Phys. Plasmas 28 022308

[13] Agullo O., et al. et al 2017 Phys. Plasmas 24 042308

[14] Candy J. 2005 Phys. Plasmas 12, 072307

[15] Ida K., et al., Phys. Rev. Letts. 100, 045003 (2008)